Self-Assembled Charge Conduits

DOI: 10.1002/ange.201309335

Photodriven Charge Separation and Transport in Self-Assembled Zinc Tetrabenzotetraphenylporphyrin and Perylenediimide Charge Conduits**

*Vladimir V. Roznyatovskiy, Raanan Carmieli, Scott M. Dyar, Kristen E. Brown, and Michael R. Wasielewski**

Abstract: *Zinc tetrabenzotetraphenyl porphyrin (ZnTBTPP) covalently attached to four perylenediimide (PDI) acceptors self-assembles into a π-stacked, segregated columnar structure, as indicated by small- and wide-angle X-ray scattering. Photoexcitation of ZnTBTPP rapidly produces a long-lived electron–hole pair having a 26 Å average separation distance, which is much longer than if the pair is confined within the covalent monomer. This implies that the charges are mobile within their respective segregated ZnTBTPP and PDI charge conduits.*

The photoactive molecules used in artificial photosynthetic systems for solar fuel production and in organic photovoltaics (OPVs) for solar electricity generation require significant molecular order to achieve high performance. The design and synthesis of complex covalent molecular systems comprising chromophores, electron donors, and electron acceptors, which mimic both the light-harvesting and the charge separation functions of photosynthetic proteins, have been demonstrated.[1] However, the development of analogous self-ordering and self-assembling components is still in its early stages.[2] We are currently developing covalently bound donor–acceptor building blocks that self-assemble into π-stacked segregated hole and electron charge conduits. These systems are designed to undergo rapid, efficient photoinduced charge separation leading to long-lived radical ion pairs (RPs, electron-hole pairs) within the covalent building block. If RP charge recombination is slow relative to hole and electron hopping between the respective non-covalent π-stacked segregated donors and acceptors in the assembly, then efficient long distance charge transport to catalysts or electrodes can be achieved.

In these studies, we have made extensive use of perylene-3,4:9,10-bis(dicarboximide) (PDI) and its derivatives, which have attracted great interest as visible chromophores for energy and charge transport studies,[1c,3] especially with regard to potential applications as visible light-absorbing electron acceptors in organic photovoltaics.[4] Not only are PDIs thermally and photochemically stable,[5] they also exhibit a strong propensity to self-organize into ordered assemblies, both in solution and in the solid state, by π–π stacking interactions, which are often aided by hydrogen bonding and nano-/micro-segregation.[1c,3] For example, we have examined a symmetrically substituted PDI acceptor (A), in which two donor groups, aminopyrene (D_1) and *p*-diaminobenzene (D_2) were coupled to the PDI through its imide positions, producing a covalent D_2–D_1–A–D_1–D_2 system.[6] This molecule self-assembles into a helical hexameric structure in methylcyclohexane solution, which upon photoexcitation undergoes two-step, sequential electron transfer to form a long-lived ion pair state, $D_2^{\bullet+}$–D_1-$A^{\bullet-}$–D_1–D_2, in which the electron migrates rapidly through the π-stacked PDIs.[6] The helical aggregate structure allows for π-stacking of the core PDI acceptors, but prevents the donors from π-stacking, so that the $D_2^{\bullet+}$ cation is trapped on a single molecule.

Zinc porphyrins have been shown to π-stack, especially when they bear substituents designed to induce discotic columnar phases, resulting in significantly enhanced hole mobilities.[7] We have previously described assemblies having a zinc *meso*-tetraphenyl-porphyrin (ZnTPP) donor core surrounded by four PDI acceptors.[8] Unfortunately, these assemblies do not have sufficiently long $ZnTPP^{\bullet+}$–$PDI^{\bullet-}$ lifetimes to allow a definitive determination of whether charge hopping between π-stacked layers is competitive with charge recombination. Compared to ZnTPP, benzannulated porphyrins, such as zinc tetrabenzotetraphenylporphyrin (ZnTBTPP), have a greater tendency to aggregate, lower oxidation potentials,[9] and red-shifted absorption spectra that provide extended solar spectral coverage.[10] Recently, benzannulated porphyrins have been exploited in high performance OPVs.[11] Herein we present molecule **1**, which has a central ZnTBTPP electron donor to which four PDI electron acceptors are linked by xylyl–phenyl spacers. The synthesis of **1** is detailed in the Supporting Information. Briefly, condensation of PDI-derived aldehyde **2** and dihydroisoindole **3** to form the octahydro precursor of **1** (Scheme 1) was followed by DDQ oxidation and metalation to furnish the ZnTBTPP core of **1**.[10] Aldehyde **2** was prepared by Suzuki coupling of 4-formylphenylboronic acid with bromophenyl PDI **4**, which in turn was obtained from condensation of **5** and 4-bromo-2,5-dimethylaniline in molten

[*] Dr. V. V. Roznyatovskiy, Dr. R. Carmieli, S. M. Dyar, K. E. Brown, Prof. M. R. Wasielewski
Department of Chemistry and Argonne Northwestern Solar Energy Research Center (ANSER), Northwestern University
2145 Sheridan Road, Evanston, IL 60208 (USA)
E-mail: m-wasielewski@northwestern.edu

[**] This work is supported by the Chemical Sciences, Geosciences, and Biosciences Division, Office of Basic Energy Sciences, DOE under grant no. DE-FG02-99ER14999.

Supporting information for this article, including detailed information about the sample preparation, electrochemistry, transient absorption spectroscopy, and TREPR spectroscopy, is available on the WWW under http://dx.doi.org/10.1002/anie.201309335.

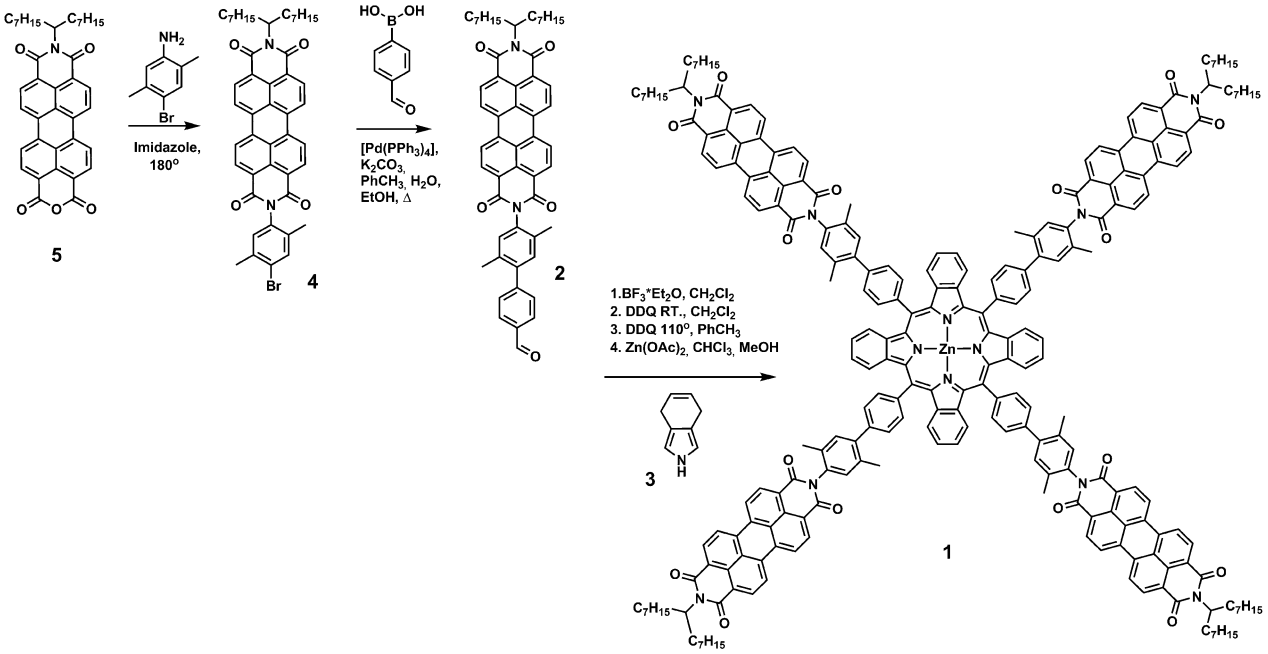

Scheme 1. Synthesis and structure of **1**.

imidazole. Dihydroisoindole **3** was prepared in several steps starting from 1,4-cyclohexadiene using the Barton–Zart method.[12]

Steady-state UV/Vis absorption spectra of **1** in toluene display strong PDI (0,0) and (0,1) vibronic absorption bands at 530 and 492 nm, respectively, and the ZnTBTPP Soret and Q_y bands at 460 and 650 nm, respectively (Figure 1). The wavelengths of these bands closely match those of the individual dyes (Supporting Information, Figure S5 and Ref. [13b]), indicating that the donor and acceptor are electronically distinct; however, the intensities of all the bands are concentration-dependent, as seen in the normalized spectra (Figure S6). The inversion in the relative intensities of the 0–0 and 0–1 transitions of PDI from lower to higher concentrations of **1** is typical for H aggregates that exhibit significant exciton coupling between the π-stacked chromophores.[13] The oscillator strengths of the ZnTBTPP Soret and Q_y bands in the spectrum of **1** also increase upon dilution, additionally suggesting a strong tendency of **1** to aggregate at concentrations greater than about 10^{-6} M. While the spectra indicate that π-stacking is occurring, they do not provide more detailed structural information.

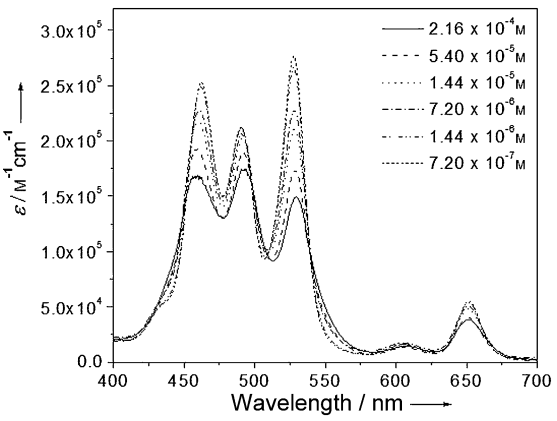

Figure 1. Absorption spectrum of **1** recorded in toluene at different concentrations at 295 K.

Additional evidence of aggregation comes from variable-temperature ^{1}H NMR spectroscopy, which reveals strong intermolecular association of **1** in [D_4]-1,2-dichlorobenzene noticeable even at elevated temperatures, although some of the resonances are better resolved at 130 °C (Figures S1, S2). The presence of large aggregates of **1** is also evident in its MALDI-TOF mass spectra, indicating the formation of higher-mass oligomers (Figure S3). The common strategy of using pyridine as an axial ligand on Zn porphyrins to inhibit aggregation has no effect on **1** in toluene, as indicated by its NMR or UV/Vis steady-state spectra.

SAXS/WAXS measurements serve as a powerful method for elucidating the solution-phase structures of non-covalent aggregates.[14] Guinier analysis of the scattering data provides, at a minimum, the radius of gyration of the complex, R_g, an estimate of its molecular weight (provided appropriate standards are available), and a gauge of the polydispersity of the aggregates.[15] In cases where the assemblies are nearly monodisperse, further analysis of the SAXS/WAXS data using atomic pair distance distribution functions (PDFs) and/or simulated annealing procedures can be performed to obtain the structure in solution with a resolution approaching 3–4 Å for molecular weights up to about 50 kD.[15b] For example, using these techniques we have previously obtained structures of complex arylene diimide assemblies having molecular weights up to about 28 kD.[6,14] The ability to carry out structural studies on such assemblies in solution at concentrations typical of time-resolved optical and EPR

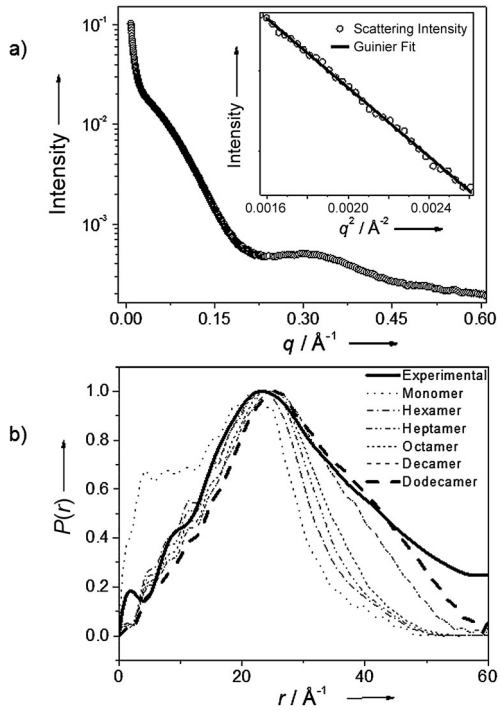

Figure 2. a) Scattering data in toluene (10^{-4} M). Inset: low-q region with Guinier fit of **1**. b) Pair distribution functions (PDFs) comparing experimental data of **1** in toluene with theoretical data generated from model structures.

spectroscopic measurements provides an important connection relating structure to function.

Figure 2a shows a logarithmic plot of scattering intensity versus q, and the inset in Figure 2a demonstrates a linear Guinier relationship of logarithmic plot of scattering intensity versus q^2 for the $0.040 < q < 0.050$ Å^{-1} range as expressed by $I(q) = I_o \exp(-q^2 R_g^2/3)$, where I_o is the forward scattering amplitude, R_g is the radius of gyration, and $q = (4\pi/\lambda)\sin\theta$ (λ is the X-ray scattering wavelength, and 2θ is the scattering angle).[15a] The observed linear Guinier relationship is indicative of the assembly having a fairly narrow size dispersity and yields a mean radius of gyration of $R_g = 23.5 \pm 0.1$ Å.[15] Energy-minimized structural models of **1** were generated using MM+ force field calculations.[14] PDFs were calculated for the experimental data and for the structural models; the latter were then varied until a best fit with the experimental PDF was found. Figure 2b compares the experimental PDF data with those of model structures that showed the closest fit. The experimental PDF differs markedly from those of smaller model aggregates and specifically from monomeric **1**. While the experimental PDF is most closely modeled by a cofacial dodecamer (**1_{12}**), it is important to note that the assembly/disassembly of this supramolecular structure is a dynamic process.[16] The **1_{12}** structure is most likely in equilibrium with a narrow distribution of similarly sized structures. The geometry-optimized π-stacked structure of **1_{12}** has a slight intermolecular twist that results in overall helicity of the aggregate, yet this helicity does not disrupt the individual ZnTBTPP and PDI π stacks (Figure 3). Not surprisingly, such behavior is common[8b] and can be rationalized in terms of the

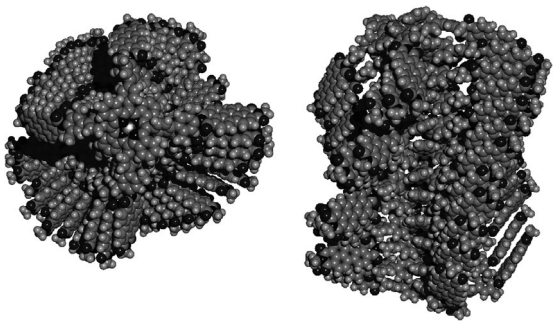

Figure 3. MM+ optimized structure of **1_{12}** that yields the best fit to the experimental SAXS/WAXS data. Two orthogonal views of the model are shown. Alkyl chains are substituted by methyl groups for clarity.

different π–π intermolecular distances required for optimal PDI-PDI and ZnTBTPP-ZnTBTPP association within the segregated stacks.[17] The SAXS/WAXS experiments show that **1_{12}** dominates at the 10^{-4}–10^{-5} M concentrations typical of the photophysical experiments presented herein, so that their observed behavior can be directly related to assembly structure.

Selective photoexcitation of ZnTBTPP in **1_{12}** (2.3×10^{-5} M) in toluene at 295 K with a 650 nm, 60 fs laser pulse results in the transient absorption spectra shown in Figure 4a. The spectra show instrument-limited bleaches of the ZnTBTPP Soret and Q_y bands followed by the rapid bleach of the PDI ground state absorption and the concomitant appearance of

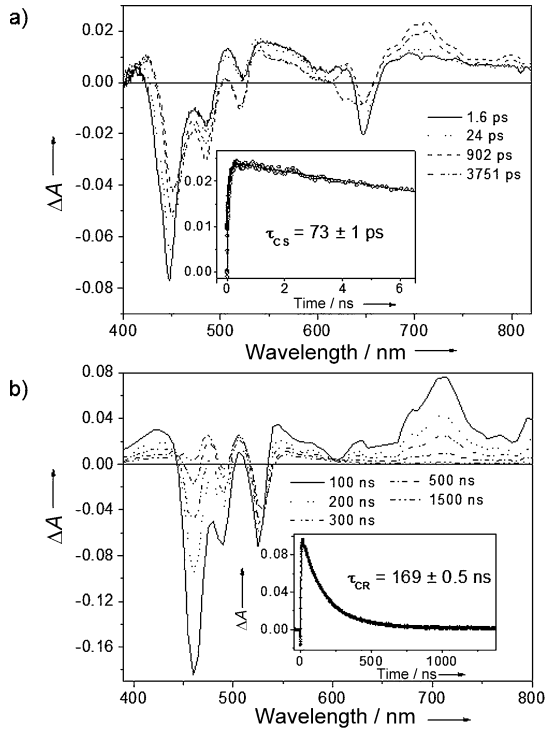

Figure 4. Transient absorption spectra of **1_{12}** (2.3×10^{-5} M) in toluene at 295 K. a) Following a 650 nm 60 fs laser pulse. Inset: transient kinetics monitored at 710 nm. b) Following a 650 nm 7 ns laser pulse. Inset: transient kinetics monitored at 710 nm.

the 710 nm PDI$^{\bullet-}$ absorption band[18] with $\tau_{CS} = 73 \pm 5$ ps. Given that the lifetime of ^{1}*ZnTBTPP in toluene is $\tau_S = 291 \pm 7$ ps (Figure S7), charge separation in $\mathbf{1_{12}}$ occurs with an 80% yield. The free energy of the charge separation reaction is $\Delta G_{CS} = -0.37$ eV as determined from the 1.89 eV lowest excited singlet state energy of ZnTBTPP and the 1.52 eV energy of the ZnTBTPP$^{\bullet+}$–PDI$^{\bullet-}$ RP (see the Supporting Information). A similar charge separation time constant is obtained from fitting the transient data following excitation of $\mathbf{1_{12}}$ at 525 nm in toluene solution at 295 K. In this case, selective excitation of PDI is followed by a rapid singlet energy transfer from ^{1}*PDI to ZnTBTPP in $\tau = 3.9 \pm 0.1$ ps followed by charge separation in $\tau_{CS} = 80 \pm 5$ ps, as monitored by formation of the PDI$^{\bullet-}$ absorption band (Figure S8). The corresponding nanosecond transient absorption spectra and kinetics (Figure 4b) show that the lifetime of ZnTBTPP$^{\bullet+}$–PDI$^{\bullet-}$ is $\tau_{CR} = 169 \pm 0.5$ ns. Our previous experience has shown that it is very difficult to produce a Zn porphyrin with four covalently-attached PDIs that does not aggregate even when disaggregating groups are purposely appended to the PDIs.[8a] However, nanosecond transient absorption measurements on **1** at 100 times lower concentration (2.2×10^{-7} M), where the equilibrium is strongly shifted toward the monomer (Figure 1), show that the lifetime of ZnTBTPP$^{\bullet+}$–PDI$^{\bullet-}$ lifetime drops to $\tau_{CR} = 63 \pm 9$ ns (Figure S9). The τ_{CR} value for predominantly monomeric **1** is substantially shorter than τ_{CR} for $\mathbf{1_{12}}$, which strongly suggests that the ZnTBTPP$^{\bullet+}$–PDI$^{\bullet-}$ distance is longer in the aggregate.

TREPR spectroscopy was used to determine the ZnTBTPP$^{\bullet+}$–PDI$^{\bullet-}$ distance within $\mathbf{1_{12}}$ and to probe the competition between charge recombination and charge transport. Following rapid charge separation, the initially formed spin-correlated singlet RP, ^{1}(ZnTBTPP$^{\bullet+}$–PDI$^{\bullet-}$) may undergo radical-pair intersystem crossing (RP-ISC)[19] to produce the triplet RP, ^{3}(ZnTBTPP$^{\bullet+}$–PDI$^{\bullet-}$). Application of a magnetic field results in Zeeman splitting of the ^{3}(ZnTBTPP$^{\bullet+}$–PDI$^{\bullet-}$) triplet sublevels, which are best described by the $|T_{+1}\rangle$, $|T_0\rangle$, and $|T_{-1}\rangle$ eigenstates that are quantized along the applied magnetic field direction, while ^{1}(ZnTBTPP$^{\bullet+}$–PDI$^{\bullet-}$) is described by the $|S\rangle$ eigenstate (Figure 5a).[19,22] The energy difference between $|S\rangle$ and $|T_0\rangle$ is the spin-spin exchange interaction $2J$, which is assumed to be isotropic. The distance dependence of $J = J_0 e^{-\beta(r-r_0)}$, where J_0 is defined at the van der Waals contact distance r_0 and r is the RP distance. In addition, for large molecules in solution, such as $\mathbf{1_{12}}$, and for molecules in the solid state, the anisotropic spin–spin magnetic dipolar coupling (d) is not rotationally averaged to zero, where $d = -2786\ \text{mT Å}\, r^{-3}$ in the point-dipole approximation.[20] The subsequent RP charge recombination process is spin selective; that is, ^{1}(ZnTBTPP$^{\bullet+}$–PDI$^{\bullet-}$) recombines to the singlet ground state, while ^{3}(ZnTBTPP$^{\bullet+}$–PDI$^{\bullet-}$) recombines to the neutral triplet state ^{3}(ZnTBTPP–PDI).[21]

When the RP distances are greater than about 15 Å, both J and d are very small relative to the magnetic fields typical of EPR spectroscopy (ca. 350 mT), so that the field invariant $|S\rangle$ and $|T_0\rangle$ states mix to produce coherent superposition states $|S'\rangle$ and $|T'\rangle$ (Figure 5b), which both have triplet character and are exclusively populated.[19,22] Microwave-induced $\Delta m = \pm 1$ transitions between these mixed states and the pure $|T_{+1}\rangle$ and $|T_{-1}\rangle$ states result in a spin-polarized EPR spectrum with four equal intensity lines having a symmetric (*e*,*a*,*e*,*a*) anti-phase pattern (where *e* denotes emission and *a* denotes enhanced absorption, low to high field), if $J > 0$ and $J > |d|$. If the g factors of the two spins are similar and/or are split by hyperfine couplings, the two doublets will overlap strongly and will often appear as a somewhat distorted (*e*,*a*) signal.[19,22]

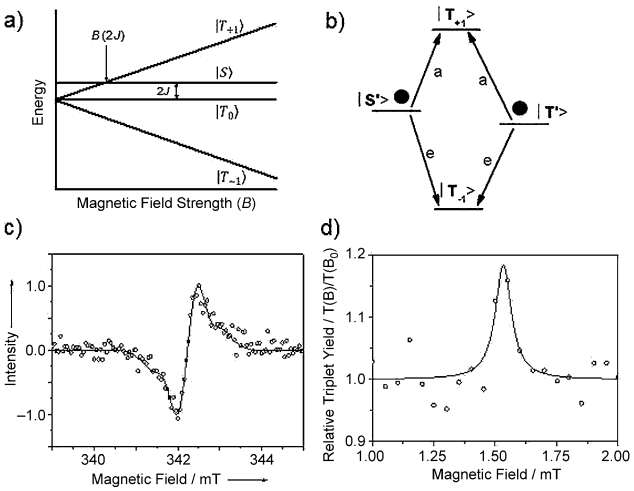

Figure 5. a) Zeeman splitting of RP energy levels. b) Initial spin population following S–T_0 mixing. c) TREPR spectrum of $\mathbf{1_{12}}$ recorded in toluene at 295 K and 100 ns following a 7 ns 532 nm laser pulse. The superimposed solid trace is a simulation of the spectrum. d) MFE data of 2.2×10^{-7} M **1** in toluene showing the $B(2J)$ resonance and a Lorenztian line fit to the data.

Photoexcitation of $\mathbf{1_{12}}$ in toluene solution with a 532 nm 7 ns laser pulse at 295 K gives a spin-polarized RP signal (Figure 5c). Simulation of this signal using the spin-correlated radical pair model[19,22] gives $J = 0.65 \pm 0.01$ mT and $d = -0.17$ mT. The average RP distance obtained from d is 26 Å. The MM+ computed molecular structure of **1** yields a center-to-center ZnTBTPP-PDI distance of 17 Å, which is much shorter than the RP distance obtained from the TREPR data on $\mathbf{1_{12}}$. This distance increase shows that charge transport occurs through the π-stacked ZnTBTPP-PDI$_4$ moieties in $\mathbf{1_{12}}$ with the 26 Å RP distance, placing ZnTBTPP$^{\bullet+}$ and PDI$^{\bullet-}$ on average about six monomers apart within the stack.

When the concentration of **1** is lowered 100-fold to 2.2×10^{-7} M, no TREPR signal is observed, even after extensive signal averaging. For molecules similar in size to monomeric **1**, we have previously observed that molecular tumbling is sufficiently rapid that the RP dipolar interaction is averaged to zero.[6] However, as J depends exponentially on distance and the spin-polarized EPR transition intensities depend on $1/J^2$,[19,22] confining the RP within the monomer (where the RP distance is only 17 Å) should result in a much larger J value and thus no observable TREPR signal. Owing to the spin-selective nature of RP charge recombination, large J values can often be measured directly using the magnetic field dependence of the resulting neutral triplet yield.[21] This dependence exhibits a resonance as the triplet yield increases at the crossing point of the $|S\rangle$ and $|T_0\rangle$ energy levels

(Figure 5a). We used nanosecond transient absorption spectroscopy to measure J directly for 2.2×10^{-7} M **1** by observing a resonance at $2J = 153$ mT (Figure 5d), so that J is 118 times larger than that of the RP in $\mathbf{1}_{12}$. Using the 17 Å and 26 Å RP distances in **1** and $\mathbf{1}_{12}$, respectively, the corresponding measured J values, and the fact that $J = J_0 e^{-\beta(r-r_0)}$, yields $\langle\beta\rangle = 0.6$, which is nicely bracketed by the β values measured for RPs separated by poly(*p*-phenylene) chains ($\beta = 0.46$)[21] and those of non-covalently π-stacked RPs ($\beta = 0.9$),[23] consistent with the proposed charge transport pathway within the self-assembled structure.

In summary, both the long-lived charge separation in the segregated π-stacks of ZnTBTPP-PDI_4 and the ability of the charges to migrate through the self-assembled structure show that the charge conduit strategy is a promising approach to improved molecular order without sacrificing solution processing in molecular materials targeting both artificial photosynthesis and OPVs.

Received: October 25, 2013
Revised: December 10, 2013
Published online: February 19, 2014

Keywords: charge separation · charge transport · donor–acceptor systems · organic photovoltaics · radical pairs

[1] a) N. Martín, L. Sánchez, M. Ángeles Herranz, B. Illescas, D. M. Guldi, *Acc. Chem. Res.* **2007**, *40*, 1015 – 1024; b) D. Gust, T. A. Moore, A. L. Moore, *Acc. Chem. Res.* **2009**, *42*, 1890 – 1898; c) M. R. Wasielewski, *Acc. Chem. Res.* **2009**, *42*, 1910 – 1921.

[2] a) G. Sforazzini, R. Turdean, N. Sakai, S. Matile, *Chem. Sci.* **2013**, *4*, 1847 – 1851; b) R. Charvet, Y. Yamamoto, T. Sasaki, J. Kim, K. Kato, M. Takata, A. Saeki, S. Seki, T. Aida, *J. Am. Chem. Soc.* **2012**, *134*, 2524 – 2527; c) L. Schmidt-Mende, A. Fechtenkötter, K. Müllen, E. Moons, R. H. Friend, J. D. MacKenzie, *Science* **2001**, *293*, 1119 – 1122.

[3] a) F. Würthner, *Chem. Commun.* **2004**, 1564 – 1579; b) F. Würthner, T. E. Kaiser, C. R. Saha-Moeller, *Angew. Chem.* **2011**, *123*, 3436 – 3473; *Angew. Chem. Int. Ed.* **2011**, *50*, 3376 – 3410.

[4] X. Zhan, A. Facchetti, S. Barlow, T. J. Marks, M. A. Ratner, M. R. Wasielewski, S. R. Marder, *Adv. Mater.* **2011**, *23*, 268 – 284.

[5] a) W. Herbst, K. Hunger, *Industrial organic pigments: production, properties, applications*, 2nd ed., Wiley-VCH, Weinheim, **1997**; b) A. Rademacher, S. Maerkle, H. Langhals, *Chem. Ber.* **1982**, *115*, 2927 – 2934.

[6] J. E. Bullock, R. Carmieli, S. M. Mickley, J. Vura-Weis, M. R. Wasielewski, *J. Am. Chem. Soc.* **2009**, *131*, 11919 – 11929.

[7] a) B. A. Gregg, M. A. Fox, A. J. Bard, *J. Am. Chem. Soc.* **1989**, *111*, 3024 – 3029; b) Y. Yuan, B. A. Gregg, M. F. Lawrence, *J. Mater. Res.* **2000**, *15*, 2494 – 2498.

[8] a) T. van der Boom, R. T. Hayes, Y. Zhao, P. J. Bushard, E. A. Weiss, M. R. Wasielewski, *J. Am. Chem. Soc.* **2002**, *124*, 9582 – 9590; b) M. J. Ahrens, R. F. Kelley, Z. E. X. Dance, M. R. Wasielewski, *Phys. Chem. Chem. Phys.* **2007**, *9*, 1469 – 1478.

[9] M. W. Renner, R.-J. Cheng, C. K. Chang, J. Fajer, *J. Phys. Chem.* **1990**, *94*, 8508 – 8511.

[10] M. A. Filatov, A. V. Cheprakov, I. P. Beletskaya, *Eur. J. Org. Chem.* **2007**, 3468 – 3475.

[11] Y. Matsuo, Y. Sato, T. Niinomi, I. Soga, H. Tanaka, E. Nakamura, *J. Am. Chem. Soc.* **2009**, *131*, 16048 – 16050.

[12] V. V. Roznyatovskiy, The University of Texas at Austin, **2011**.

[13] a) M. Kasha, H. R. Rawls, M. Ashraf El-Bayoumi, *Pure Appl. Chem.* **1965**, *11*, 371 – 392; b) J. M. Giaimo, J. V. Lockard, L. E. Sinks, A. M. Scott, T. M. Wilson, M. R. Wasielewski, *J. Phys. Chem. A* **2008**, *112*, 2322 – 2330.

[14] a) D. M. Tiede, R. Zhang, L. X. Chen, L. Yu, J. S. Lindsey, *J. Am. Chem. Soc.* **2004**, *126*, 14054 – 14062; b) M. J. Ahrens, L. E. Sinks, B. Rybtchinski, W. Liu, B. Jones, J. M. Gaimo, A. V. Gusev, A. J. Goshe, D. M. Tiede, M. R. Wasielewski, *J. Am. Chem. Soc.* **2004**, *126*, 8284 – 8294; c) X. Y. Li, L. E. Sinks, B. Rybtchinski, M. R. Wasielewski, *J. Am. Chem. Soc.* **2004**, *126*, 10810 – 10811; d) Y.-L. Wu, K. E. Brown, M. R. Wasielewski, *J. Am. Chem. Soc.* **2013**, *135*, 13322 – 13325.

[15] a) A. Guinier, G. Fournet, *Small-Angle Scattering of X-rays*, Wiley, New York, **1955**; b) D. I. Svergun, M. H. Koch, *Rep. Prog. Phys.* **2003**, *66*, 1735 – 1782.

[16] Z. Chen, U. Baumeister, C. Tschierske, F. Würthner, *Chem. Eur. J.* **2007**, *13*, 450 – 465.

[17] a) M. P. Byrn, C. J. Curtis, Y. Hsiou, S. I. Khan, P. A. Sawin, S. K. Tendick, A. Terzis, C. E. Strouse, *J. Am. Chem. Soc.* **1993**, *115*, 9480 – 9497; b) O. S. Finikova, A. V. Cheprakov, P. J. Carroll, S. Dalosto, S. A. Vinogradov, *Inorg. Chem.* **2002**, *41*, 6944 – 6946.

[18] D. Gosztola, M. P. Niemczyk, W. Svec, A. S. Lukas, M. R. Wasielewski, *J. Phys. Chem. A* **2000**, *104*, 6545 – 6551.

[19] G. L. Closs, M. D. E. Forbes, J. R. Norris, *J. Phys. Chem.* **1987**, *91*, 3592 – 3599.

[20] O. Efimova, P. J. Hore, *Biophys. J.* **2008**, *94*, 1565 – 1574.

[21] a) E. A. Weiss, M. J. Ahrens, L. E. Sinks, A. V. Gusev, M. A. Ratner, M. R. Wasielewski, *J. Am. Chem. Soc.* **2004**, *126*, 5577 – 5584.

[22] U. Till, P. J. Hore, *Mol. Phys.* **1997**, *90*, 289 – 296.

[23] F. D. Lewis, T. Wu, Y. Zhang, R. L. Letsinger, S. R. Greenfield, M. R. Wasielewski, *Science* **1997**, *277*, 673 – 676.

